Journal of Applied Fluid Mechanics, Vol. 18, No. 4, pp. 904-918, 2025.
Available online at www.jafmonline.net, ISSN 1735-3572, EISSN 1735-3645.
https://doi.org/10.47176/jafm.18.4.2924

Study of Stage Gap for a 2-bladed 2-stage Savonius-like-hydro-kinetic Turbine Performance Involving End Plates and Overlapping

K. C. Sarma, B. Nath†, A. Biswas and R. D. Misra

Department of Mechanical Engineering, National Institute of Technology Silchar, Assam, India

†*Corresponding Author Email: biswajit21_rs@mech.nits.ac.in*

ABSTRACT

Savonius-like-hydrokinetic turbine (SLHT) is a revelation for small-scale (micro/pico) power generation from perennial rivers at low water velocities and low tip speed conditions. However, for its operation at such sites, efficiency is to be improved by design modifications and flow control. This work entails a flow control strategy that combines the mean flow with overlapping flow, gap flow between stages, and flow between end plates. Here, the performance of a two-bladed two stage SLHT with end plates and 15% blade overlapping is examined in a water channel with stage gaps in mm (0-20), low water velocities in m/s (0.45-0.65) under applied braking loads in g (100-1500). The results demonstrate that SLHT produces more power and torque under a low-stage gap as the brake load rises, reaching the highest hydrodynamic torque (0.056 Nm) during a maximum load of 1250 g. The minimal stage gap is 5 mm, turbine braking loading 1250 g, 0.248 TSR, and 0.55 m/s water velocity yield the highest power coefficient (0.058), which is greater than some published SLHT designs. Thus, as much as blade profile modifications, flow control through SLHT can be the future direction for further improvement of its performance.

Article History

Received June 21, 2024
Revised October 21, 2024
Accepted October 29, 2024
Available online February 4, 2025

Keywords:

Savonius-like-hydrokinetic turbine
Turbine loading
Power coefficient
Torque coefficient
Water velocity
Gap between stages
Overlapping
End plates

1. INTRODUCTION

Renewable Energy has become a necessary resource for the socio-economic development of a nation. Due to rapid industrialization and shifting of load centers in urban locations, energy consumption on per capita basis is ever-increasing (Wang et al., 2019; Abbasi et al., 2021; Perez et al., 2021). Due to heightened reliance on energy, the demand and consumption, environmental impacts, and cost of energy have been rising over the years (Shahsavari and Akbari, 2018; Healy et al., 2019; Perez et al. 2021). Also, the flow patterns in different terrains and atmospheric conditions have direct implications on the turbine performance and thus the harness of energy (Han et al., 2018; Wang et al., 2022, 2023). Freely flowing low-stream hydro reserves can be implemented on hydrokinetic energy converters to produce green energy economically. Such hydrokinetic converters or turbines can absorb available energy from rivers, irrigation and manmade channels, canals, and flumes to produce power in an isolated, small-scale manner (Solangi et al., 2019; Ibrahim et al., 2020; Quaranta and Davies, 2022). Also, the hydrokinetic turbine, which can be installed particularly in locations far from electrical grids, has immense prospects for electrical power generation from free-stream water currents (Elbatran et al., 2021; Sarma et al., 2023).

One type of hydrokinetic turbine for low-stream applications is SLHT. This technique offers a novel and inventive method for producing electricity in low-velocity flow reserves (Alizadeh et al., 2020; Sinsel et al., 2020; Sarma et al., 2022). In addition, it is a machine capable of harnessing drag force for its operation. With SLHT blades, the turbine's self-starting is flawless. It features a very simple blade profile when contested with more complicated airfoil-blade designs, such as troposkein-type Darrieus turbines (Bazooyar and Darabkhani 2020; Sahebzadeh et al.2020; Zhang et al. 2021).

SLHT, which exhibit a difference in pressure between the two sides of the rotor blades, produce self-spinning for capturing the kinetic energy of moving water (Thakur et al., 2019). The water speed in low stream reserves is characteristically low, so is the blade tip speed causing the exhibition of SLHT's low efficiency (Mohammadi et al., 2018; Quaranta et al., 2020; Ridgill et al., 2021). In such a situation, an effective approach would be to utilize the low-flow stream in a better manner by exerting more water thrust, e.g., by multi-staging (Frikha et al., 2016), blade profile modifications, conduits, nozzles, and similar flow guides (Sari et al., 2018; Tiwari et al., 2020). The problem

of subdued efficiency of SLHT is also attended by previous researchers by focusing on end plates to increase water pressure on blades (Shashikumar ., & Madav 2021; Shashikumar et al., 2021a) by overlapping to increase water pressure (Thiyagaraj et al., 2023), by completely replacing semi-circular blade profile with elliptical, twisted, and multiple of such blades (Mauro et al., 2019), using deflectors (Chaudhari and Shah 2023), etc. The below discussions entail some of the prominent research outcomes on the Savonius turbine in line with the problem as identified. (Chemengich et al., 2022) investigated the double gap flow guides of a Savonius turbine at various angular orientations and displayed a maximum increase of power coefficient by 12.24% at 75º angular orientation and 0.4 m/s. The impact of twisted blades of a Savonius turbine mounted on a vertical shaft with direct flow control features was investigated by (Tahani et al., 2017). The results demonstrated that a twist-bladed Savonius design showed a betterment of the power coefficient by 18%. Khan et al. (2022) created a unique blade curvature (a section of an S1048 airfoil) for SLHT and showed a power coefficient of 14%. Shamsuddin and Kamaruddin (2023) observed that second-stage blades in two-stage turbine had improved flow regulation at larger water velocity due to the vertical velocity gradient, reaching the highest power coefficient (C_p) of 0.104. Kumar et al. (2020) investigated the performance of a modified Savonius hydro-kinetic turbine involving a twisted blade along with several stages. According to their study, a double-stage turbine having water-velocity of 0.38 m/s can achieve a maximum power coefficient of 0.44, which corresponds to a tip speed ratio (TSR) value of 0.9. To improve the performance further, a new model was developed by using the NACA series Savonius blade profile along with end plates (Yosry et al., 2021). From the numerical study, it was found that Cp reached 0.25 with TSR 1.52 for the lowest upstream speed of 0.33 m/s. Jeon et al. (2015) numerically analyzed the Savonius turbine using helical blades with end plates. The results revealed that both lower and upper-end plates enhanced C_p by more than 36%. Osama et al. (2024) developed a Savonius turbine using a hydrofoil blade profile to enhance its performance. Their results demonstrated that the hydrofoil profile achieved the highest coefficient of power 0.26 for 140° camber angle with a water-velocity of 0.4 m/s and an overlapping ratio of 0.15. The influence of aspect ratio and overlapping ratio in a Savonius turbine was investigated by (Patel et al., 2017) to enhance its hydrodynamic performances. When the aspect ratio of Savonius turbines was less than 0.6, the maximum coefficient of power was observed at an overlapping ratio of 0.11. Two deflectors in upstream as augmentation devices for enhancing the power of the triple-bladed traditional Savonius turbine (ST) were used by Salleh et al. (2021). The results reported a maximum C_p of 0.183. Salleh et al. (2020) increased the power performance of the Savonius turbine by adjusting the longitudinal-position ratios of deflectors. The maximum C_p, 0.26, was achieved by the turbine. Moshabi et al. (2021) used combined deflector plates in Savonius design along with blade twist and performed experiments in an irrigation channel. The design achieved a maximum C_p of 0.166. Mosbahi et al. (2020) experimented on a Savonius turbine in an irrigation channel with an innovative akin to Savonius blade having sweeping elements at its leading edge. The greatest value of C_p was 0.184 for water velocity of 0.86 m/s. Tapered and standard Savonius turbine blades for the production of hydel power were examined by (Shashikumar et al., 2021b). The outcome indicated that the slanted blade boosted the outcome of the traditional turbine by 5%. Savonius turbine efficiency was also increased through several other enhancement methods, by the application of porous deflector resulting in the highest C_p of 0.274 for a water velocity 0.7 m/s and TSR=1 (Nimvari et al., 2020); wind booster (wind velocity=1-8m/s, C_p = 0.977) (Korprasertsak and Leephakpreeda, 2016) and nozzle duct (C_p = 0.25, TSR = 0.73) (Elbatran et al., 2017).

Sarma et al. (2022, 2023) recently investigated two-stage configurations of two/three-bladed SLHT to improve SLHT performance at low velocity conditions (0.4-0.6) m/s. They considered a new parameter called stage gap between stages (Sarma et al., 2022, 2023) and combined with 15% blade overlapping (Sarma et al. 2023) to investigate SLHT's performance. The power performance of SLHT was shown to be strongly influenced by the stage gap between the stages and blade overlapping for the gap flow and overlapping flow, respectively.

However, in these works, the contribution of end plates on the turbine ends was not investigated. This will further result in flow control between end plates, causing water pounding and thus further raising pressure on the turbine blades. Thus, the combination of end plates, stage gaps, and blade overlapping (15%) can be an effective flow control method along with the mean flow for raising SLHT performance in such low water velocity and low blade tip-speed ratio conditions. Therefore, the current experimental inquiry is carried out on a two-bladed two-stage SLHT to study the effect of stage gaps (0-20 mm, in a span of 5 mm) along with end plates and with 15% blade overlapping under low water velocity of 0.45-0.65 m/s. Additionally, the contribution of turbine brake loads, 100-1500 g, on the functionality of the present SLHT has also been enumerated. Further, to provide useful performance insights, complete turbine performances at different off-design and design scenarios are explored. Thus, this unique work is the simultaneous applications of three flow control measures (i.e. overlapping flow, gap flow, and flow between end plates) along with mean flow control for raising the two-bladed two-stage SLHT's performance.

2. DESIGN OF TURBINE AND EXPERIMENTATION

The present two-bladed two-stage SLHT, along with end plates with stage gap (G = 0,5, 10, 15, and 20) mm adjoining the stages, were fabricated. The stage gap, top view, and front view are depicted in Fig. 1 (a-c). The two-bladed turbine stages are spanned at 90° from each other and mounted on a co-axial vertical shaft (Diameter = 0.014 m). Each of the turbine blades is 1.5 mm thick (material aluminum) and was fabricated from a circular cylinder in the form of semi-circular halves with a 0.14 m chord

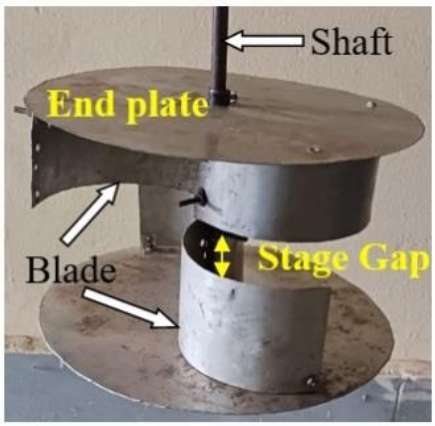

(a)

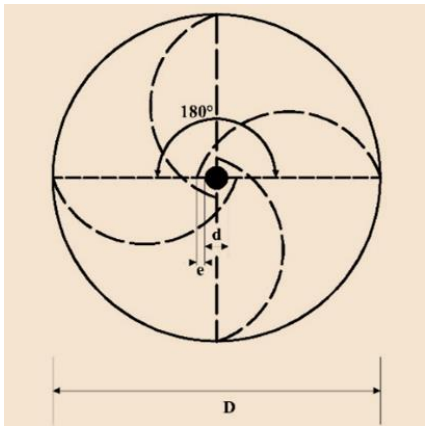

(b)

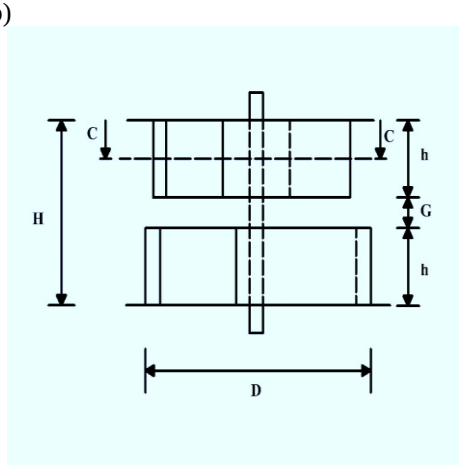

(c)

Fig. 1 (a) Actual fabricated design; (b) turbine top view; and (c) turbine front view

distance and length of 0.085 m. Thus, each two-bladed staging height is 0.085 m with an overall 0.26 m diameter for any stage. The two end plates at the ends of the two-stage turbine have a diameter of 0.286 m, as shown in Table 1 Therefore, the resultant turbine height is 0.17 m (for no stage gap condition). However, as the stage gap between the stages increases up to 20 mm, starting from 0 mm in 5 mm increments, the aspect ratio also increases as 0.65, 0.67, 0.69, 0.71, and 0.73 for the increase of height of the SLHT. From the literature, it is seen that the maximum C_p of the Savonius rotor can be obtained in the case of 0.7 aspect ratio (Mosbahi et al. 2020). Thus, the present height/diameter ratio of the resultant double-stage two-bladed turbine is close to the benchmarked aspect

Table 1 Specification of present turbine

Particulars	Present modified SLHT
Turbine diameter (D)	0.260 m
Diameter of End plates	0.286 m
Turbine height (H_T)	0.17 m
Shaft diameter (d)	0.014 m
Blade Thickness (t)	1.5 mm
No. of blades (n)	2
Overlapping ($2e/D$)	15%
Stage gap (G)	0,5,10,15 and 20 mm

ratio condition, thereby validating the design. The tests were carried out inside open channel at a range of low water-velocity (0.45 to 0.65) m/s and under a range of turbine brake load conditions (100-1500 g) following standard practices.

During operation in the water currents of an open channel, the turbine assembly on the co-axial shaft was supported with a ball-bearing mounted on a sturdy flat frame, and the assembly of the two-bladed turbines was kept fully submerged during the course of experiments. The experimental picture with a schematic of the system is depicted in Fig. 2 (a-b). The upper surface of the fabricated SLHT models has been fully immersed inside the open channel (made by: Zephyr Enterprise, India) flow during experiments. Test channel height 0.505 m, width 0.9 m, and 12 m length. The highest water channel depth is 0.24 m with corresponding discharge is 91 L/s. As per requirements, the water depth was regulated by controlling discharge gate. Two centrifugal pumps were used in the channel arrangement for delivering water across the open- channel: the first pump, made by Kirloskar Brothers Ltd., 15 hp rating, and the second, made by Crompton Greaves Ltd., 20 hp rating. In addition, a third pump with a capacity of 25 hp was seldom used to get the maximum immersion of the turbine assembly in the water.

The water from the underground reservoir were circulated by pumps through the open channel. The water tank holds the necessary water for circulation. In this channel, the maximum obtained water velocity is 0.65 in m/s, which is recorded by a device known as an Acoustic Doppler Velocimeter (ADV), also known as a water current meter with an accuracy of 1%, for measuring instantaneous water velocities at any point at a sampling rate of 0.09-49Hz. Therefore, in this work, water velocity is termed as water velocity, whereas its meaning and unit are the same as water velocity.

The present ADV measures the speeds of the water current in the range of 0.03-2.5m/s, which covers the considered water velocity of this study. The water velocity data recorded by the ADV probe were delivered via a computer interface for the record. Also, to record the blade speed of the turbine in revolutions per minute, a contactless digital sensor called a tachometer (make-Systems, accuracy 1%) was used in the test system. Each reading is repeated at least five times, and average value is calculated. This is done to minimize errors from different sources, like voltage fluctuations, human error,

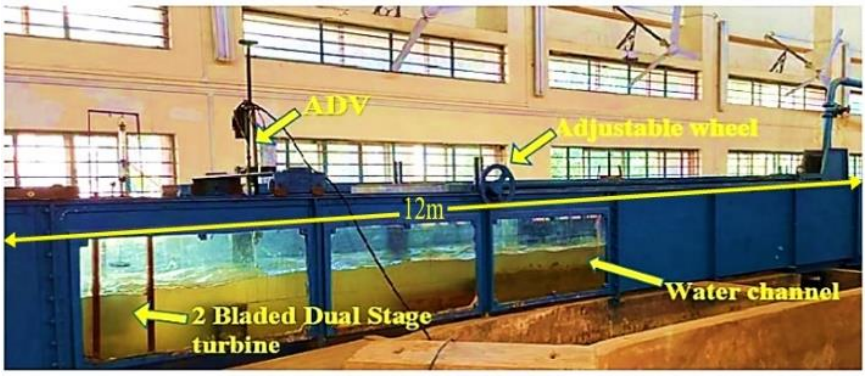

(a)

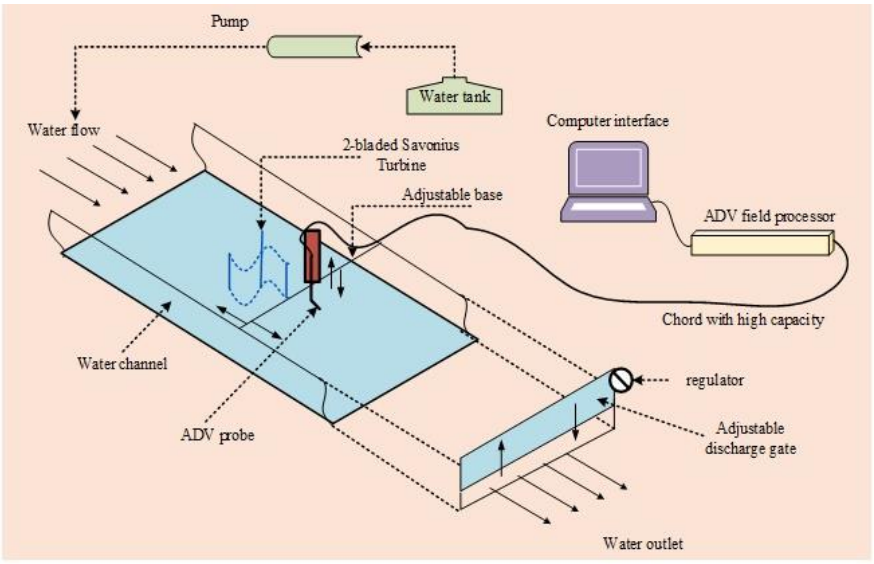

(b)

Fig. 2 (a) Photograph of the open channel flume (b) Schematic representation of the test rig and the setup

and other chance causes of errors. The present design of the turbine and the test system is part of an Indian Patent, which is registered and published (Application No.202331055032 A).

In this study, the developed two-bladed, two-stage SLHT with a height-to-diameter ratio of 0.65 is studied for various gap distances between the stages.

2.1 Mathematical Expressions

Using free-stream water current or water velocity (V), the maximum water power (P_{max}) for free-flow stream water speed *V* is obtained from eq. 1 (Modi et al., 1984) as

$$P_{max} = \frac{1}{2}\rho A V^3 \quad (1)$$

'ρ'- water density, '*A*'-turbine swept area.

'T'- torque (Nm) is determined by the load by the rope-brake dynamometer is obtained from eq. 2 (Wu et al., 2012) as

$$T = \frac{(L_a - R_s)(S_R + R_{ns})g}{1000} \quad (2)$$

'R_s' and 'L_a' represent the spring balance reading and applied load, respectively, the shaft radius is denoted by S_R, and the radius of string (make- nylon) is denoted as $R_{n.s}$. The power generated by the SLHT is obtained from eq. 3 (Modi et al., 1984; Wu et al., 2012) as-

$$P = \tau\omega \quad (3)$$

'ω'- turbine's circular frequency of rotation. As such, the effect of parasitic drag due to ball bearing is ignored in the present work as being negligible, considering the present operating conditions. The power coefficient (C_p), which is the ratio of power extracted by the turbine to the maximum water power, is obtained from eq.4 (Modi et al., 1984; Wu et al., 2012) as-

$$C_P = \frac{P}{P_{max}} \quad (4)$$

Torque coefficient (C_T) is expressed in Eq. (5) (Wu et al., 2012) as:

$$C_T = \frac{T}{0.5\rho A V^2 R} \quad (5)$$

'R' represents the radius of the turbine in 'm'.

Tip-speed-ratio (*TSR*) is the ratio of the product of the circular frequency of rotation and turbine radius to the free-flow stream water speed, and it is obtained from eq. 6 (Kirke 2011) as-

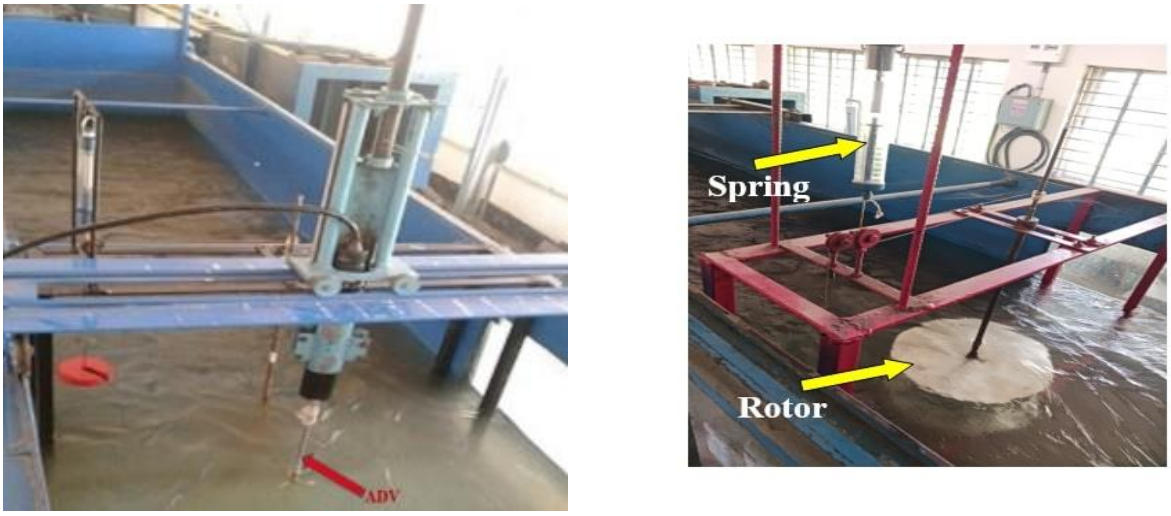

(a) (b

Fig. 3 (a) Arrangement of the test rig with rope-brake dynamometer and turbine and (b) Setting of the ADV probe in the upstream flow

$$TSR = \frac{\omega R}{V} \quad (6)$$

Further, the intensity of turbulence (T_{int}) to understand the flow situation at any point in the channel flow is also estimated from eq. 7 (Saha and Rajkumar 2006; Bartl et al., 2012) as-

$$T_{int} = \left(\frac{1}{\bar{v}}\right)\sqrt{\frac{1}{3}\left(x'^2 + y'^2 + z'^2\right)} \quad (7)$$

x′, y′, and z′ represent the velocity fluctuations along three directions. Turbulence intensity is required to be less than 1% to ensure a more streamlined flow and also to judge the behavior of the SLHT. Based on the locations of minimum turbulence in the flow channel, the turbine can be suitably placed, which will also ensure its stable function. In the present experimental conditions, it has been noted that placing the turbine test rig at a distance of 9.4 m downstream of the water supply pumps resulted in a minimum turbulence intensity of 0.15%; so, this is an acceptable level for its stable operation. Furthermore, in the operation of the turbine, there should not be any blockage effect, which can modify the flow velocities in the channel. So, blockage ratio (β) can be defined as the turbine's swept area (H × D) to the channel's section area ($H_{ch} \times W_{ch}$), and it is obtained from eq. 8 (Munson et al. 1995) as

$$\beta = \frac{H \times D}{H_{ch} \times W_{ch}} \quad (8)$$

Turbine height is H, turbine diameter is D, channel height up to which water is there is H_{ch}, and channel width is W_{ch}. The present maximum blockage ratio is found to be 21.38 % (i.e., less than 30%), for which no blockage correction was required as per the work of (Alexander and Holownia 1978). As free-flow stream water speed varies from one water depth to another, the water speed is required to be computed for different depths, with a bed of the channel taken as the datum. In this work, water speeds were checked at water depths of 0.07 m, 0.09 m, and 0.14 m, where, with the help of the ADV probe, the data were collected and recorded in a computer interface. The mean water velocity in the channel in the range of 0.4 m/s to 0.6 m/s. Further, the turbine's top edge was submerged at least 0.02 m below the free surface. The water velocity data were received from the ADV setup at distances of 0.28 m and 0.35 m from the axis of the turbine, and then the mean of the readings was considered in the calculations. This way of recording was maintained for both upstream and downstream locations.

Different test readings are recorded in order to ensure consistency of the measurement. Additionally, to assure a simple process for capturing data reduction, errors resulting from uncertainties and voltage fluctuations during tests are recorded; thus, the accuracy of the data acquired is measured. The arrangement of the rope-brake dynamometer and setting of the ADV probe in the upstream flow is shown in Fig. 3(a) and (b).

The representation of the open channel in schematic form with various recording points for the ADV probe is provided in Fig. 4, which shows various upstream locations along the channel and also locations from the channel's right and left sidewalls. The measuring points denote a pitch distance of 5 cm between them. This arrangement depicts the various locations where water velocity was measured to judge the flow uniformity of the channel by measuring the flow distributions at these locations. The velocity distributions at these locations were measured across different water depths of the channel. In this work, the distributions at the middle layer of water in the channel were reported as a case of flow uniformity study.

2.2 Error Estimation

All measuring instruments have errors owing to their traceability at the time of calibration, so this is to be estimated during experimentation. Thus the instrumental errors are estimated from eq.9 as-

$$\lambda_T = ((\lambda_{Tm})^2 + (\lambda_{ADV})^2 + (\lambda_{SB})^2)^{0.5} \quad (9)$$

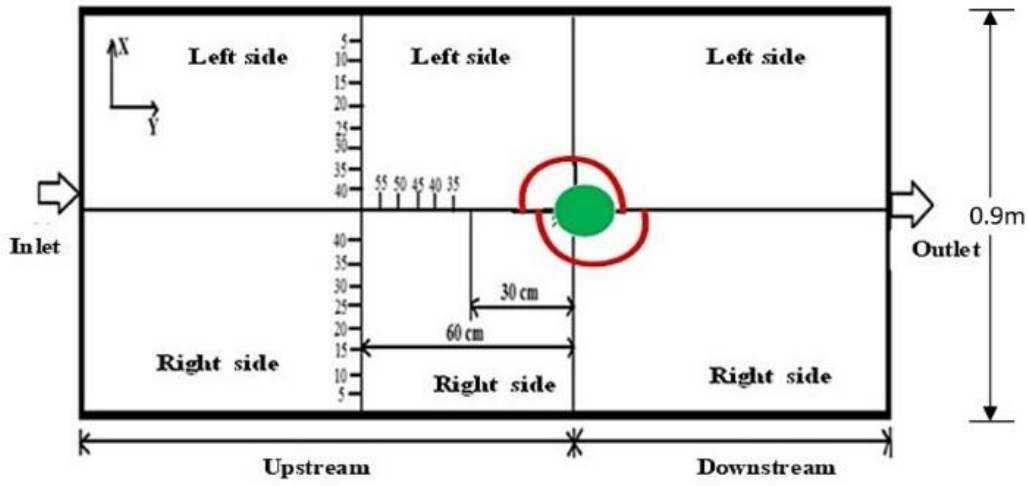

Fig. 4 Representation of various measuring points in the channel for flow uniformity

Table 2 Instruments Specifications

Particulars	Instruments name		
	ADV	Tachometer (rpm sensor)	Spring Balance
Accuracy	±1%	± 2%	±0.25%
Range of values	0.36±0.01m/s	16 ± 0.02 rpm	0.496 ±0.0025 N
Error %	2.77%	0.125%	0.504%

where, λ_T means total error percentage, λ_{Tm} means the error in the rpm sensor, i.e. tachometer, λ_{ADV} means ADV's error, and λ_{SB} means error in spring balance reading at the time of loading of the turbine.

The instrumental errors result in the uncertainty of the measured performance parameters, i.e., C_p and hydrodynamic torque (τ). Thus, the maximum C_p error is computed using an uncertainty equation as depicted in eq.10 and the same in hydrodynamic torque as depicted in eq. 11.

$$\frac{\delta C_{power}}{C_{power}} = \sqrt{\left(\frac{\delta\tau}{\tau}\right)^2 + \left(\frac{\delta w}{w}\right)^2 + \left(3\frac{\delta V}{V}\right)^2} \quad (10)$$

$$\frac{\delta\tau}{\tau} = \frac{\delta R_S}{R_S} \quad (11)$$

The necessary specifications of all the measuring instruments are provided in Table 2. The resultant uncertainties of C_p and τ are enumerated as ± 3.61% and ± 0.25%, respectively.

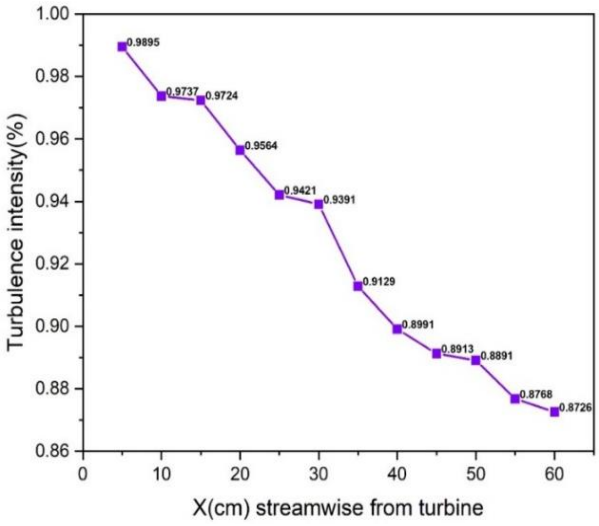

Fig. 5 Turbulence Intensity of overall RMSE 0.14% by measuring at different stream-wise points from the turbine

3. EXPERIMENTATION RESULTS

The experimental findings are deliberated in this section, which is divided into two major subsections, i.e. maintained test conditions for best practices for assessing the turbine performance and the outcomes of the experiments on the turbine.

3.1 Maintained Test Conditions

The liquid flow in the channel should have the least amount of turbulence possible. As shown in Fig. 5, the visualized water velocity is monitored in steps of 5 cm from 5 to 60 cm from the turbine axis to assess upstream turbulence intensities with the help of Eq. 6. The measured turbulence intensity values are shown in Fig. 5. The ADV probe positioned at different locations (as per Fig.4) detected the mean velocities and variations of the mean velocities in three directions. Then, these mean velocities and their fluctuations are substituted in Eq.6 to estimate the values of turbulence intensities at various points in the flow direction. Root mean square (RMS) error in the variations of turbulence intensity resulted in 0.14%, which can be considered to be acceptable. Further observation reveals that as the gap (5 to 60 cm) increases towards the upstream direction, the turbulence intensities gradually drop from 0.98% to 0.87%, indicating streamlined water

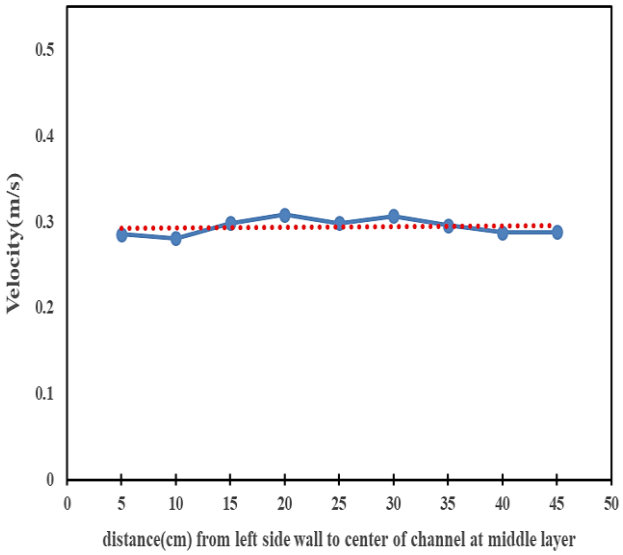

(a)

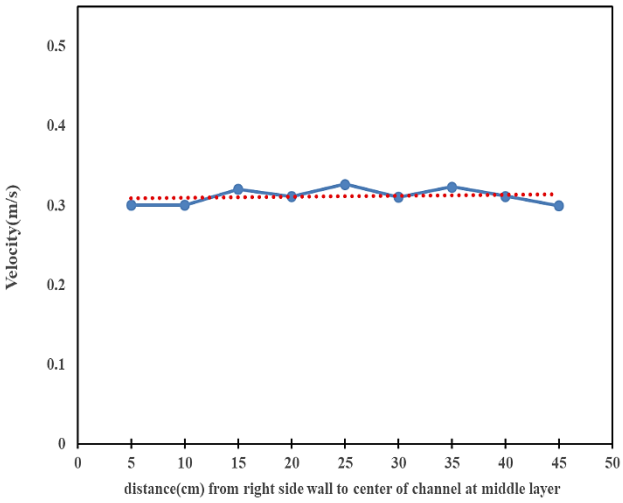

(b)

Fig. 6. Water velocity distributions off the channel sidewalls - (a) mid-layer of left sidewall and (b) mid-layer of right sidewall

flow in the vicinity of the turbine site. Due to the interplay between the incoming water current and the rotating turbine, it is anticipated that the amount of turbulence near the turbine position will rise.

Prior to starting the major trials, it is critical to reduce how much the turbine functioning is impacted by the channel's sidewall. For the purpose of evaluating flow uniformity in relation with a constant water velocity i.e. 0.55 m/s in the water flow, the middle layer of water (21 cm), or the middle of the turbine axis, is used. The distributions of water velocity that result across the turbine are therefore examined. When seen in reference to the left sidewall, the various locations towards channel's center are shown on the x-axis to mark the salient cross-stream points of measurements. Similar points in the cross-stream with water velocity measurements are also maintained with regard to the right sidewall (see Fig. 4). It is noted that the water velocity distributions at the middle water layer, as illustrated in Fig. 6, are largely uniform. Figure 6(a) and (b) show that root mean square errors of 0.04% and 0.03%, respectively, the mean water speed at the middle water layer (i.e., at a distance of 21 cm from the channel bed) is about 0.30 m/s towards right and left sidewalls of the channel from the center of the turbine. These flow uniformity tests are done to ensure that side walls do not modify the flow pattern and thus influence the turbine performance. The main tests are then carried out after seeing this homogeneity in average water speed, and the results are described in the next section.

3.2 Outcomes of the Experiments

The final tests were conducted to measure the outputs produced by the turbine after verifying uniformity of the experimental settings in the previous section. The tests were carried out inside the open channel at a range of low water-velocity (0.45 to 0.65) m/s and under a range of turbine brake load conditions (100-1500 g).

The five various arrangements of the double-blade Savonius-like turbines have stage gap requirements ranging from 0 mm to 20 mm. The effect of stage gap on the present SLHT involving end plates and 15% blade overlapping has been studied. As mentioned earlier, the end plates are fixed at the turbine ends. As such, variation of overlapping is not studied in this work, as in the previous work of the same authors on the three-blade configuration of the SLHT; the best overlapping was obtained at 15% condition by Sarma et al. (2024). The performances measured for the turbine are T(Nm), P(W), C_p, and TSR.

3.2.1 Brake Load Effect on Turbine Performance

Figure 7 depicts the fluctuations about T(Nm), P(W), C_p, and TSR with load (100–1500) g at 0.55 m/s water-velocity. When the load increases, the torque grows continuously until it reaches its peak value of up to 1250 g., which then decreases as the load increases beyond 1250g. The turbine can still generate work (or power) at 1250g, but as the load rises to 1500 g, it starts to lose efficiency. This is due to the fact that when the load is increased beyond 1250 g, turbine work and performance are reduced as a result of the decrease in turbine rpm and, consequently, TSR. Thus, regardless of flow rate and gap, TSR steadily falls as the load increases. In order to accept heavier loads on the blades, the blade speed generally decreases. Consequently, the present turbine's ideal weight cannot be maintained below 1250 g, which might cause it to function like a motor. As a result, for the gap between stages of 5 mm, a braking loading of 1250 in g, and water velocity of 0.55 m/s, highest torque (0.056) N-m is produced. Therefore, to maintain torque production under heavier loads, the water velocity and gap between stages are to be maintained at 0.55 m/s and 5mm. For different stage gap, all hydrodynamic parameter variations get better as the gap across the stages rises to 5 mm; however, as the stage gap rises above 5 mm to 20 mm, the same variations get worse. The potential reason for the performance loss might be the migration of flow through the stage gap without hitting the blades if the stage gap increases beyond 5 mm. These patterns are in line with observations that were previously reported (Sarma et al. 2022, 2023).

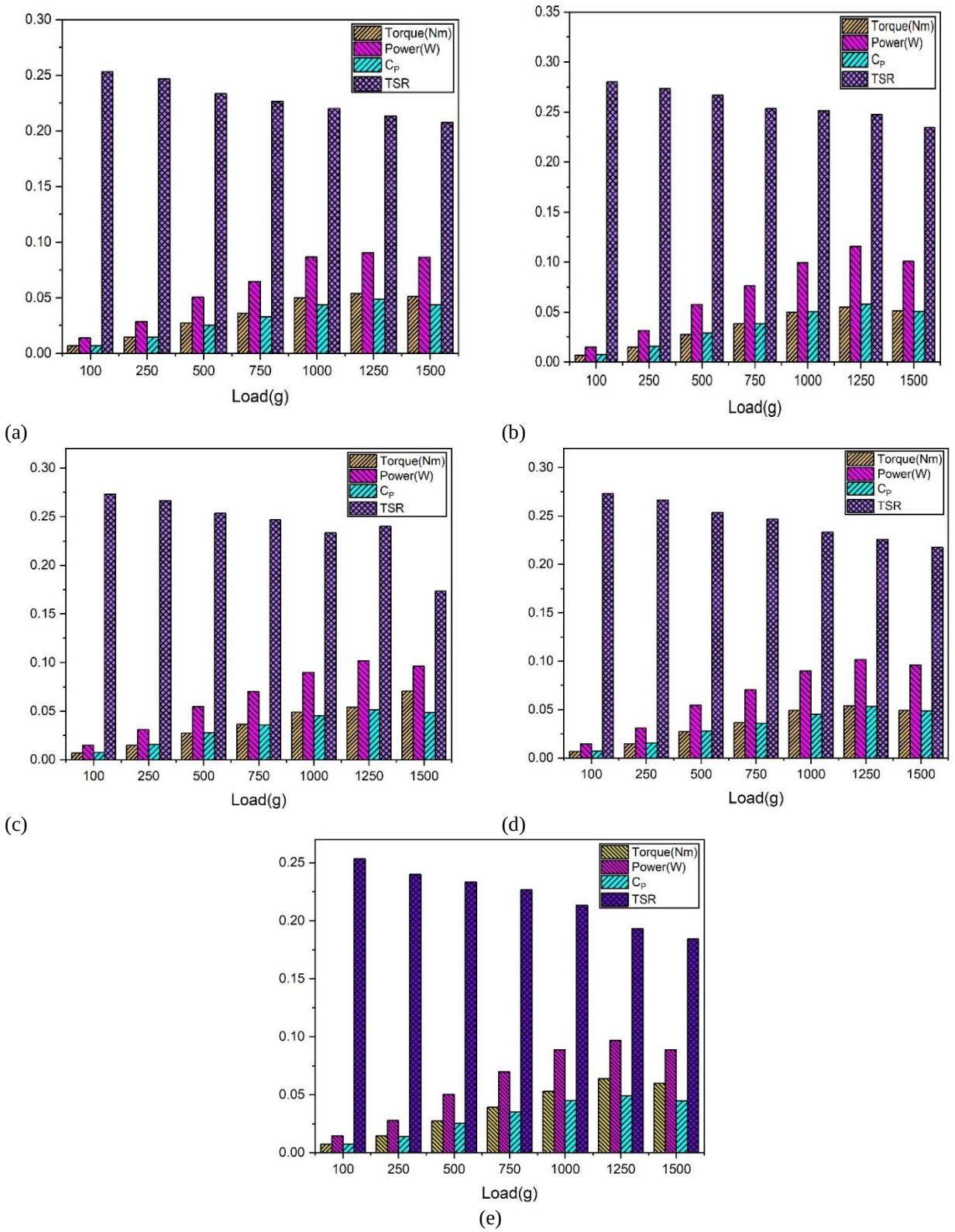

Fig. 7 Variations of torque, power, C_p, and TSR with various turbine loads at water velocity 0.55 m/s for gap across stages: (a) 0mm, (b) 5 mm, (c) 10 mm, (d) 15 mm, and (e) 20 mm

3.2.2 Effect of Water-Velocity On Turbine Performance

The results indicate that the SLHT exhibits improved power performance in the examined stage gaps and low water current conditions at 0.55 m/s for a weight of 1250 g, indicating a best load for maximum C_p.

As shown in Figs. 8(a) through (d), the values of the parameters, i.e., power, torque, C_p, and *TSR* at the considered braking load for all stage gaps, are obtained for water velocity of 0.45, 0.55, and 0.65 m/s. This is done to ascertain how water velocity impacts the turbine's hydrodynamic torque at the ideal braking load of 1250 g. For all stage gaps, Fig. 8(a) depicts the rise of turbine

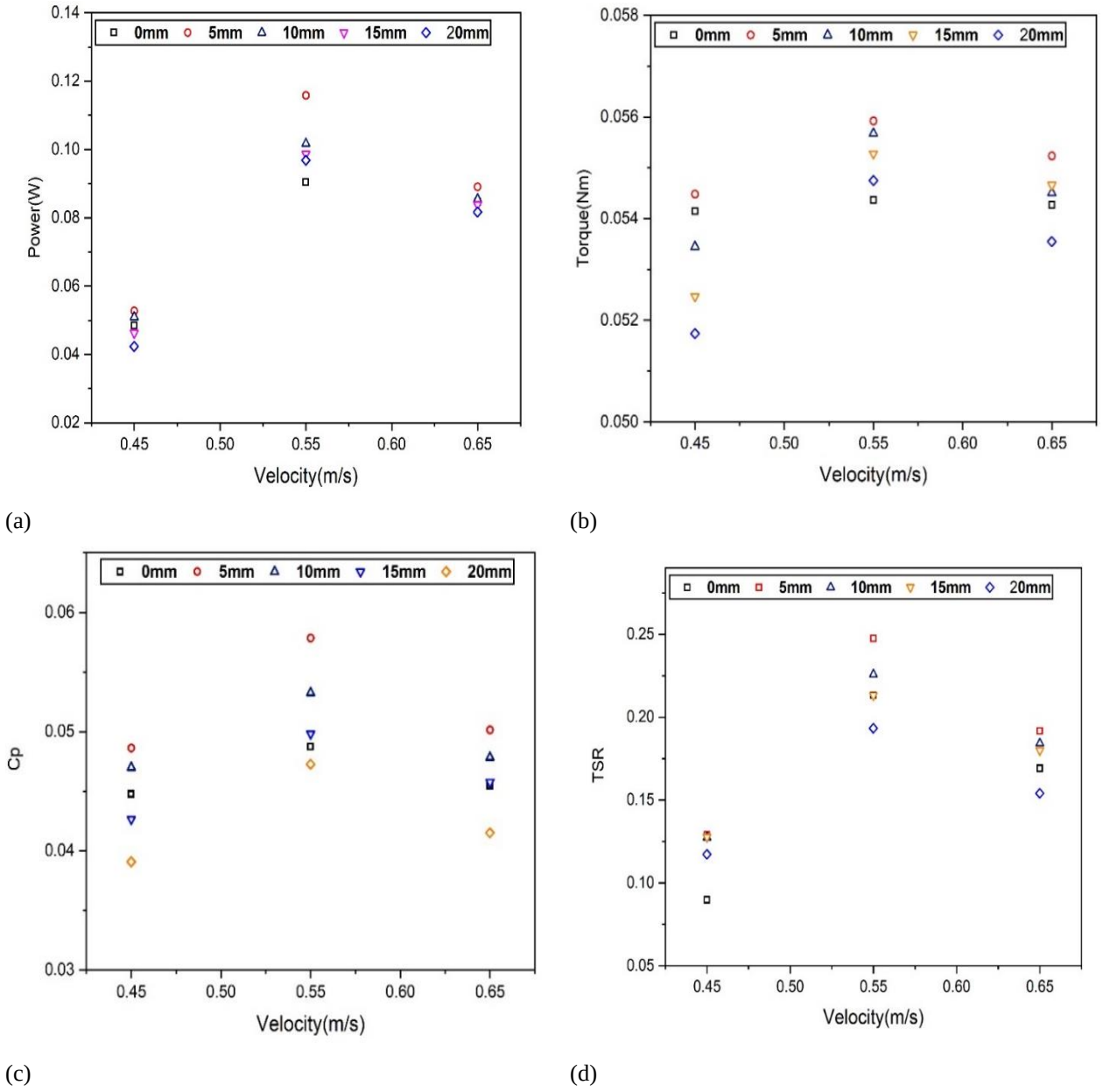

Fig. 8 (a)*P*(W), (b) *T*(Nm), (c) C_p, and (d) *TSR* at 1250g load with respect to the water velocity for the investigated gaps

power output when the water velocity reaches 0.55m/s. When the water velocity is 0.55 m/s, and the gap between the stages is 5 mm, the SLHT runs at its maximum turbine power output of 0.116 W. The torque and TSR variations show why the power of the turbine reduces with a rise in water velocity greater than 0.55 m/s at higher stage gaps (i.e.15 mm and 20 mm). Figure 8 (b) shows that at 1250 g load, torque rises when the water velocity increases to a value of 0.55 m/s, and then it decreases as the water velocity rises further. However, with stage gaps above 15 mm and water velocity beyond 0.55m/s, the torque decreases continuously, resulted in negative effect in terms of performance. The probable cause might be the effect of high water pressure on the SLHT's blades due to increased water velocity, and consequently, water passes through the higher stage gaps (resulting in a loss of volumetric discharge and loss of performance). According to Fig. 8(c), C_p improves when the water velocity reaches 0.55 m/s; however, for an increased gap across the stages of 10 mm to 20 mm, it declines continuously following the same trend of torque variation. As shown in Fig. 8(d), similar trends are observed for *TSR*, with a rise in water velocity up to 0.55m/s and a 5mm stage gap. Thus, when the results are thoroughly analyzed as described above, the advantages of retaining a gap (5 mm) and a braking load (1250 g) become evident.

Table 3 provides Power, C_p, Torque, and *TSR* for loading 1250 in g and 5 mm gap with regard to investigated water velocity (from 0.45 to 0.65) m/s to emphasize this point. Table 3 clearly shows that water-velocity of 0.45 m/s and 0.65 m/s and *TSR* of 0.129 and 0.192 are non-preferred turbine performance conditions for the current turbine design as its torque and power performances are inferior to the design operating with 0.55 m/s.

Table 3 Turbine performance results for 5.0 mm gap and 1250 g load

Water velocity (m/s)	T (Nm)	P (W)	C_p	*TSR*
0.45	0.054	0.053	0.049	0.129
0.55	**0.056**	**0.116**	**0.058**	**0.248**
0.65	0.055	0.089	0.050	0.192

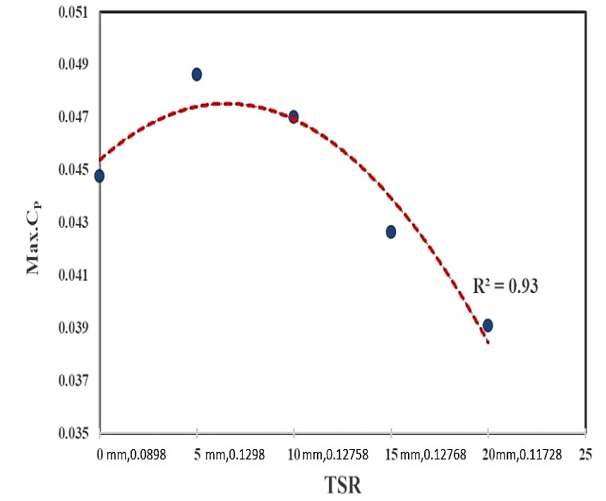

(a)

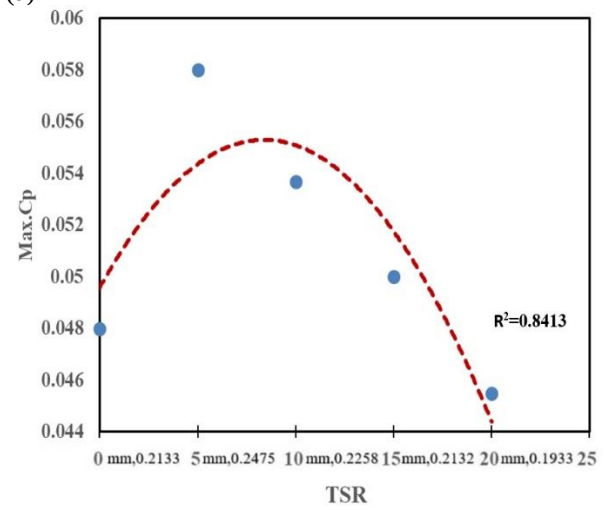

(b)

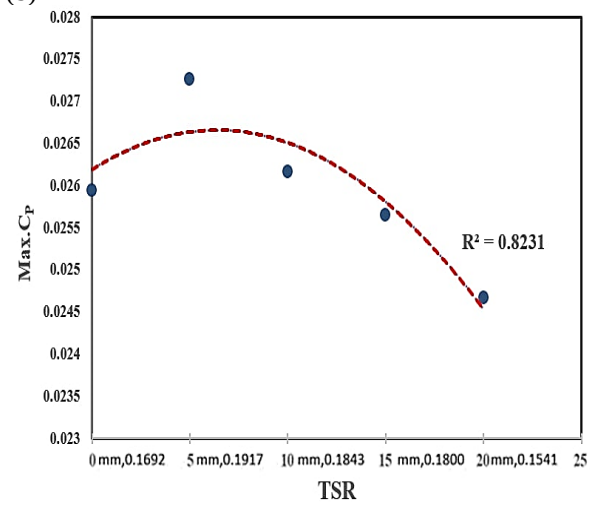

(c)

Fig. 9 Maximum C_p variation for the considered gaps at the best load against *TSR* at water velocities- 0.45 m/s (a), 0.55 m/s (b), and 0.65 m/s (c)

3.2.3 Effect of TSR and Stage Gap on Maximum C_p

The fluctuations of the SLHT's maximum C_p with TSR for water velocities 0.45-0.65 m/s are shown in Fig. 9(a-c). For each water velocity situation in subplots, the best combinations of turbine load, i.e., 1250 g, overlapping 15%, are considered. Further, in the x-axis, the gap is also shown along with the corresponding best TSR as obtained earlier. Thus, Fig. 9(a-c) illustrates the point at which highest C_p is attained, representing the SLHT's maximum performance attribute. The highest C_p of 0.058 is achieved for stage-gap (5 mm) and water-velocity (0.55 m/s) at 0.248 *TSR*, is shown in Fig. 9(b). Therefore, this best stage gap accepts maximum flow rates till 0.55 m/s and loads 1250 g, which allows maximum blade fluid interactions by exerting the most possible thrust to the blade. However, when the gap across the stages rises even further, the water passes without having an effect on the blades. Further, Fig. 9 depicts that the graphs are generated with a high value of the coefficient of correlation (i.e., R^2), justifying the validity of the data points.

3.2.4 Comparison of Maximum C_p at Best Stage Gap Of 5 mm for Different Water Velocities

The changes in maximum C_p with different water velocities (0.45,0.55 and 0.65) m/s at a 5mm gap are depicted in Fig. 10. The graph shows that the maximum *Cp* of 0.058 is obtained at a 5 mm stage gap and water velocity of 0.55m/s. The root mean square error of *Cp* is 0.01%, i.e., less than 5%, which can be considered satisfactory. The benefit of maintaining a gap of 5mm between the double-bladed two stages of SLHT with overlapping and joined end plates is clearly shown by a critical analysis of these results.

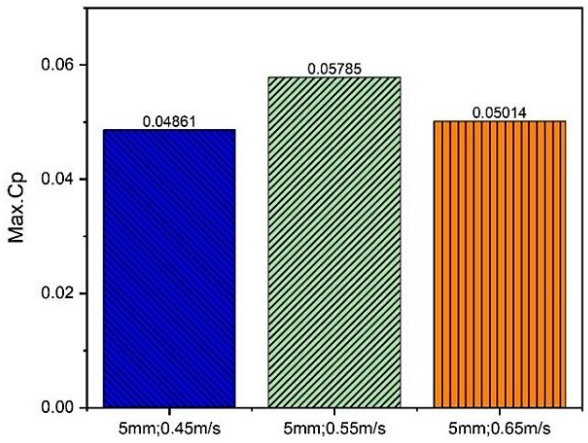

Fig. 10. Relation between maximum C_p (best gap conditions) and brake load at water-velocities (0.45, 0.55, and 0.65) m/s

Table 4 Performance comparison with some notable works

Reference	Year	Type of blades	Rotor Size D_T (mm)	Water velocity (m/s)	C_p
Khan et al. (2009)	2009	2 blades in two stage	220	1	0.029
Thiyagaraj et al. (2021)	2021	3 blades with only one stage	165	0.8	0.105
Salleh et al. (2021)	2021	3 blades with only one stage & with end plates	329	0.4	0.050
Shashikumar & Madav (2021)	2021	2 blades in single stage with end plates	72.6	0.309	0.051
Sarma et al. (2022)	2022	2-blades in two-stage	260	0.5	0.034
Present study	-	2-blades in two-stage with end plate	221	0.55	0.058

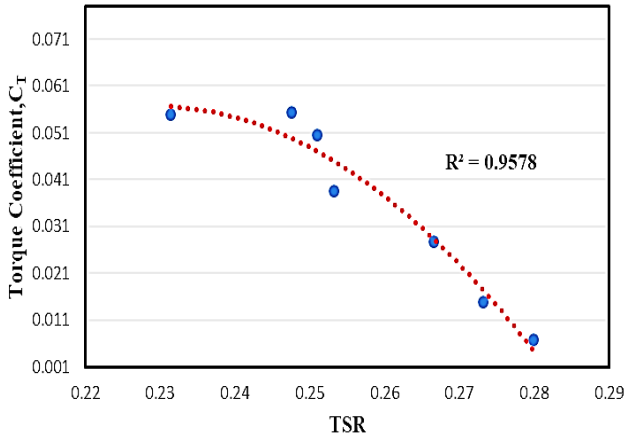

Fig. 11 Schematic of maximum C_T versus *TSR* for design operating water velocity 0.55 m/s

3.2.5 Effect of TSR on C_T with Best Water-Velocity 0.55 m/s with Gap 5 mm

Figure 11 depicts how (C_T) of the turbine at the best turbine load (1250 g) fluctuates with regard to *TSR* for water-velocity of 0.55 m/s and a best gap of 5 mm. The highest C_T of 0.055 is 0.248 TSR, and then it decreases when the TSR rises further. The same trend is also obtained in Salleh et al. (2021). The root mean square error of C_T is 0.03%, i.e. less than 5%, which can be considered satisfactory as per standard practice. The present turbine blades are able to harness maximum C_T for (0.55 m/s) velocity and a load (1250 g), which is allowable by this turbine having the best stage gap of 5 mm, and for this design condition of the turbine, it is able to produce the maximum flow thrust on its blades. Further, Fig. 11 also depicts that the coefficient of correlation is more than 95%, which is an indication of the validity of the data points.

4. COMPARISON OF PERFORMANCE OF THE PRESENT TURBINE WITH EXISTING WORKS IN LITERATURE

The objective is to determine the performance of the present turbine by comparing it with some of the notable works of the literature. For this, different existing designs using two/three-bladed, single/two-stage SLHT designs with or without end plates have been taken from the literature and highlighted in Table 4, along with the design of the present study as well. However, while comparing, it is difficult to find from literature exactly matching turbine size (diameter) and operating water velocity as that of the present case. However, an attempt has been made to compare with similar designs and operating conditions within a given range, as depicted in Table 4. The comparison elucidates that with the two-bladed configuration of the SLHT, accommodating two stages with the best gap across the stages (i.e., 5 mm) at a preferred water velocity of 0.55 m/s can exhibit either similar or higher C_p (0.058) compared to the notable works of the literature, including the work of (Sarma et al., 2022a). Further, it also shows that recent works on two-stage configurations of SLHT are quite scarce in the literature, although the two-stage configuration can exhibit better performance. Thus, this is the essence of the present work.

It is also attempted to contest the present experimental results and its variations with two prominent recent works of Salleh et al. (2021) and Shashikumar and Madav (2021) over a range of TSR, as depicted in Fig. 12. Figure 12 also elucidates that the present design exhibits a higher maximum C_p (0.058) than that of Shashikumar and Madav (2021) (i.e. 0.051) and almost the same as obtained bySalleh et al. (2021) within the similar range of operating *TSR*.

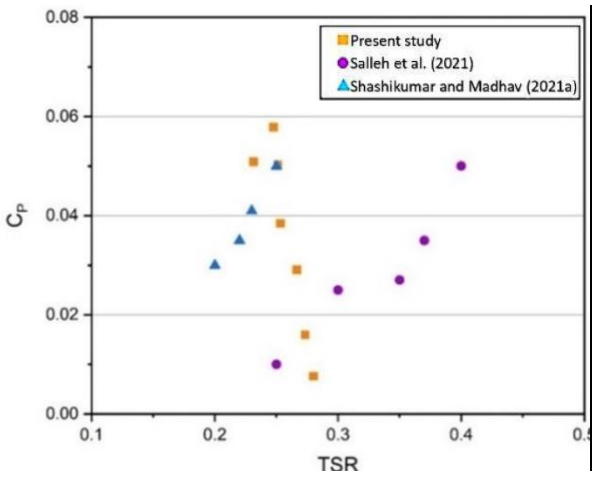

Fig.12. Comparing C_p among the present SLHT, Salleh et al. (2021) and Shashikumar & Madav (2021) vs *TSR*

5. CONCLUSIONS AND RECOMMENDATIONS

In the present research, a unique two-bladed, two-stage, end-plated Savonius-like-hydrokinetic turbine (SLHT) was investigated under different design and flow conditions to see the improvement in its performance. From the present study, the following conclusions are summarized:

- It is obtained that 5 mm is the appropriate gap for the two-bladed two-stage SLHT. It is discovered that 1250 g is the perfect brake load for maximizing the turbine's performance.
- SLHT produces more power and torque under a low gap (5 mm) as the brake load rises, reaching maximum hydrodynamic torque (0.056 Nm) at the highest load of 1250 g for a water velocity or speed 0.55 m/s and tip-speed ratio of 0.248.
- The highest power produced from the model SLHT is 0.116W for the above water velocity and tip speed conditions.
- SLHT generates its highest power coefficient and torque coefficient of 0.058 and 0.055, respectively, which, when compared to the two-bladed, double-stage SLHTs previously studied, is either improved or matched under a low operating tip-speed ratio.

One practical limitation of the study was that the experiments could not be conducted at a water velocity above one m/s, which can also be found in channels and rivers during monsoons and heavy rainfalls. For further increasing flow thrust over the blades and improvement of performance, future research may include modification of the semi-circular blade profile along with a combination of different stages and deflectors. The current 2-bladed, 2-stage Savonius hydro turbine may be set up in water channels to produce power at low water velocity of 0.55 m/s or more, allowing for better operational flexibility.

ACKNOWLEDGMENTS

The support provided by the Fluid Machinery laboratory of ME Deptt, NIT Silchar, is sincerely acknowledged.

CONFLICT OF INTEREST

The authors declare no conflict of interest.

AUTHORS CONTRIBUTION

K. C. Sarma: Conceptualization, Methodology, Formal Analysis, Investigation, Writing of the Original Draft; Review and Editing, Visualization. **B. Nath:** Methodology, Formal Analysis, and Validation. **A. Biswas:** Conceptualization, Supervision, Review, and Editing. **R. D. Misra:** Supervision, Review, and Editing.

REFERENCES

Abbasi, K. R., Abbas, J., & Tufail, M. (2021). Revisiting electricity consumption, price, and real GDP: A modified sectoral level analysis from Pakistan. *Energy Policy, 149*, 112087. https://doi.org/10.1016/j.enpol.2020.112087

Alexander, A. J., & Holownia, B. P. (1978). Wind tunnel tests on a Savonius rotor. *Journal of Wind Engineering and Industrial Aerodynamics*, *3*(4), 343-351. https://doi.org/10.1016/0167-6105(78)90037-5

Alizadeh, H., Jahangir, M. H., & Ghasempour, R. (2020). CFD-based improvement of Savonius type hydrokinetic turbine using optimized barrier at the low-speed flows. *Ocean Engineering*, *202*, 107178. https://doi.org/10.1016/j.oceaneng.2020.107178

Bartl, J., Pierella, F., & Sætrana, L. (2012). Wake measurements behind an array of two model wind turbines. *Energy Procedia*, *24*, 305-312. https://doi.org/10.1016/j.egypro.2012.06.113

Bazooyar, B., & Darabkhani, H. G. (2020). Design, manufacture and test of a micro-turbine renewable energy combustor. *Energy Conversion and Management*, *213*, 112782. https://doi.org/10.1016/j.enconman.2020.112782

Chaudhari, V. N., & Shah, S. P. (2023). Numerical investigation on the performance of an innovative Airfoil-Bladed Savonius Hydrokinetic Turbine (ABSHKT) with deflector. *International Journal of Thermofluids*, *17*, 100279. https://doi.org/10.1016/j.ijft.2023.100279

Chemengich, S. J., Kassab, S. Z., & Lotfy, E. R. (2022). Effect of the variations of the gap flow guides geometry on the savonius wind turbine performance: 2D and 3D studies. *Journal of Wind Engineering and Industrial Aerodynamics*, *222*, 104920. https://doi.org/10.1016/j.jweia.2022.104920

Elbatran, A. H. A., Yaakob, O. B., & Ahmed, Y. M. (2021). Experimental investigation of a hydraulic turbine for hydrokinetic power generation in irrigation/rainfall channels. *Journal of Marine Science and Application*, *20*, 144-155. https://link.springer.com/article/10.1007/s11804-020-00152-4

Elbatran, A. H., Ahmed, Y. M., & Shehata, A. S. (2017). Performance study of ducted nozzle Savonius water turbine, comparison with conventional Savonius turbine. *Energy*, *134*, 566-584. https://doi.org/10.1016/j.energy.2017.06.041

Frikha, S., Driss, Z., Ayadi, E., Masmoudi, Z., & Abid, M. S. (2016). Numerical and experimental characterization of multi-stage Savonius rotors. *Energy*, *114*, 382-404. https://doi.org/10.1016/j.energy.2016.08.017

Han, X., Liu, D., Xu, C., & Shen, W. Z. (2018). Atmospheric stability and topography effects on wind turbine performance and wake properties in complex

terrain. *Renewable Energy*, *126*, 640-651. https://doi.org/10.1016/j.renene.2018.03.048

Healy, N., Stephens, J. C., & Malin, S. A. (2019). Embodied energy injustices: Unveiling and politicizing the transboundary harms of fossil fuel extractivism and fossil fuel supply chains. *Energy Research & Social Science*, *48*, 219-234. https://doi.org/10.1016/j.erss.2018.09.016

Ibrahim, M. M., Mostafa, N. H., Osman, A. H., & Hesham, A. (2020). Performance analysis of a stand-alone hybrid energy system for desalination unit in Egypt. *Energy Conversion and Management*, *215*, 112941. https://doi.org/10.1016/j.enconman.2020.112941

Jeon, K. S., Jeong, J. I., Pan, J. K., & Ryu, K. W. (2015). Effects of end plates with various shapes and sizes on helical Savonius wind turbines. *Renewable Energy*, *79*, 167-176. https://doi.org/10.1016/j.renene.2014.11.035

Khan, M. N. I., Iqbal, T., Hinchey, M., & Masek, V. (2009). Performance of Savonius rotor as a water current turbine. *The Journal of Ocean Technology*, *4*(2), 71-83. https://research.library.mun.ca/235/

Khan, Z. U., Ali, Z., & Uddin, E. (2022). Performance enhancement of vertical axis hydrokinetic turbine using novel blade profile. *Renewable Energy*, *188*, 801-818. https://doi.org/10.1016/j.renene.2022.02.050

Kirke, B. K. (2011). Tests on ducted and bare helical and straight blade Darrieus hydrokinetic turbines. *Renewable Energy*, *36*(11), 3013-3022. https://doi.org/10.1016/j.renene.2011.03.036

Korprasertsak, N., & Leephakpreeda, T. (2016). Analysis and optimal design of wind boosters for Vertical Axis Wind Turbines at low wind speed. *Journal of Wind Engineering and Industrial Aerodynamics*, *159*, 9-18. https://doi.org/10.1016/j.jweia.2016.10.007

Kumar, A., Saini, R. P., Saini, G., & Dwivedi, G. (2020). Effect of number of stages on the performance characteristics of modified Savonius hydrokinetic turbine. *Ocean Engineering*, *217*, 108090. https://doi.org/10.1016/j.oceaneng.2020.108090

Mauro, S., Brusca, S., Lanzafame, R., & Messina, M. (2019). CFD modeling of a ducted Savonius wind turbine for the evaluation of the blockage effects on rotor performance. *Renewable Energy*, *141*, 28-39. https://doi.org/10.1016/j.renene.2019.03.125

Modi, V. J., Roth, N. J., & Fernando, M. S. U. K. (1984). Optimum-configuration studies and prototype design of a wind-energy-operated irrigation system. *Journal of Wind Engineering and Industrial Aerodynamics*, *16*(1), 85-96. https://doi.org/10.1016/0167-6105(84)90050-3

Mohammadi, M., Mohammadi, R., Ramadan, A., & Mohamed, M. H. (2018). Numerical investigation of performance refinement of a drag wind rotor using flow augmentation and momentum exchange optimization. *Energy*, *158*, 592-606. https://doi.org/10.1016/j.energy.2018.06.072

Mosbahi, M., Ayadi, A., Chouaibi, Y., Driss, Z., & Tucciarelli, T. (2020). Experimental and numerical investigation of the leading edge sweep angle effect on the performance of a delta blades hydrokinetic turbine. *Renewable Energy*, *162*, 1087-1103. https://doi.org/10.1016/j.renene.2020.08.105

Mosbahi, M., Elgasri, S., Lajnef, M., Mosbahi, B., & Driss, Z. (2021). Performance enhancement of a twisted Savonius hydrokinetic turbine with an upstream deflector. *International Journal of Green Energy*, *18*(1), 51-65. https://doi.org/10.1080/15435075.2020.1825444

Munson, B. R., Young, D. F., & Okiishi, T. H. (1995). Fundamentals of fluid mechanics. *Oceanographic Literature Review*, *10*(42), 831. https://www.infona.pl/resource/bwmeta1.element.elsevier-013ce2bb-5df3-353d-9205-9c4162529c62/tab/summary

Nimvari, M. E., Fatahian, H., & Fatahian, E. (2020). Performance improvement of a Savonius vertical axis wind turbine using a porous deflector. *Energy Conversion and Management*, *220*, 113062. https://doi.org/10.1016/j.enconman.2020.113062

Osama, S., Emam, M., Ookawara, S., & Ahmed, M. (2024). Enhancing the performance of vertical axis hydrokinetic Savonius turbines using a novel cambered hydrofoil profile for rotor blades. *Ocean Engineering*, *292*, 116561. https://doi.org/10.1016/j.oceaneng.2023.116561

Patel, V., Bhat, G., Eldho, T. I., & Prabhu, S. V. (2017). Influence of overlap ratio and aspect ratio on the performance of Savonius hydrokinetic turbine. *International Journal of Energy Research*, *41*(6), 829-844. https://doi.org/10.1002/er.3670

Perez, A., & Garcia-Rendon, J. J. (2021). Integration of non-conventional renewable energy and spot price of electricity: A counterfactual analysis for Colombia. *Renewable Energy*, *167*, 146-161. https://doi.org/10.1016/j.renene.2020.11.067

Quaranta, E., & Davies, P. (2022). Emerging and innovative materials for hydropower engineering applications: Turbines, bearings, sealing, dams and waterways, and ocean power. *Engineering*, *8*, 148-158. https://doi.org/10.1016/j.eng.2021.06.025

Quaranta, E., Bonjean, M., Cuvato, D., Nicolet, C., Dreyer, M., Gaspoz, A., ... & Bragato, N. (2020). Hydropower case study collection: Innovative low head and ecologically improved turbines, hydropower in existing infrastructures, hydropeaking reduction, digitalization and governing systems. *Sustainability*, *12*(21), 8873. https://doi.org/10.3390/su12218873

Ridgill, M., Neill, S. P., Lewis, M. J., Robins, P. E., & Patil, S. D. (2021). Global riverine theoretical hydrokinetic resource assessment. *Renewable Energy*, *174*, 654-665. https://doi.org/10.1016/j.renene.2021.04.109

Saha, U. K., & Rajkumar, M. J. (2006). On the performance analysis of Savonius rotor with twisted blades. *Renewable Energy*, *31*(11), 1776-1788. https://doi.org/10.1016/j.renene.2005.08.030

Sahebzadeh, S., Rezaeiha, A., & Montazeri, H. (2020). Towards optimal layout design of vertical-axis wind-turbine farms: Double rotor arrangements. *Energy Conversion and Management*, *226*, 113527. https://doi.org/10.1016/j.enconman.2020.113527

Salleh, M. B., Kamaruddin, N. M., & Mohamed-Kassim, Z. (2020). The effects of deflector longitudinal position and height on the power performance of a conventional Savonius turbine. *Energy Conversion and Management*, *226*, 113584. https://doi.org/10.1016/j.enconman.2020.113584

Salleh, M. B., Kamaruddin, N. M., Mohamed-Kassim, Z., & Bakar, E. A. (2021). Experimental investigation on the characterization of self-starting capability of a 3-bladed Savonius hydrokinetic turbine using deflector plates. *Ocean Engineering*, *228*, 108950. https://doi.org/10.1016/j.oceaneng.2021.108950

Sari, M. A., Badruzzaman, M., Cherchi, C., Swindle, M., Ajami, N., & Jacangelo, J. G. (2018). Recent innovations and trends in in-conduit hydropower technologies and their applications in water distribution systems. *Journal of Environmental Management*, *228*, 416-428. https://doi.org/10.1016/j.jenvman.2018.08.078

Sarma, K. C., Biswas, A., & Misra, R. D. (2022). Experimental investigation of a two-bladed double stage Savonius-akin hydrokinetic turbine at low flow velocity conditions. *Renewable Energy*, *187*, 958-973. https://doi.org/10.1016/j.renene.2022.02.011

Sarma, K. C., Biswas, A., Nath, B., & Misra, R. D. (2024). Effect of overlapping and space between stages of a three-bladed double-stage Savonius hydrokinetic turbine for low flow speed perennial river application. *Energy Sources, Part A: Recovery, Utilization, and Environmental Effects*, *46*(1), 1177-1195. https://doi.org/10.1080/15567036.2023.2295521

Sarma, K. C., Nath, B., Biswas, A., & Misra, R. D. (2023). Design and performance investigation of a triple blade dual stage Savonius-alike hydrokinetic turbine from low flow stream reserves. *Energy Sources, Part A: Recovery, Utilization, and Environmental Effects*, *45*(4), 12099-12117. https://doi.org/10.1080/15567036.2023.2268572

Shahsavari, A., & Akbari, M. (2018). Potential of solar energy in developing countries for reducing energy-related emissions. *Renewable and Sustainable Energy Reviews*, *90*, 275-291. https://doi.org/10.1016/j.rser.2018.03.065

Shamsuddin, M. S. M., & Kamaruddin, N. M. (2023). Experimental study on the characterization of the self-starting capability of a single and double-stage Savonius turbine. *Results in Engineering*, *17*, 100854. https://doi.org/10.1016/j.rineng.2022.100854

Shashikumar, C. M., & Madav, V. (2021). Numerical and experimental investigation of modified V-shaped turbine blades for hydrokinetic energy generation. *Renewable Energy*, *177*, 1170-1197. https://doi.org/10.1016/j.renene.2021.05.086

Shashikumar, C. M., Honnasiddaiah, R., Hindasageri, V., & Madav, V. (2021a). Studies on application of vertical axis hydro turbine for sustainable power generation in irrigation channels with different bed slopes. *Renewable Energy*, *163*, 845-857. https://doi.org/10.1016/j.renene.2020.09.015

Shashikumar, C. M., Vijaykumar, H., & Vasudeva, M. (2021b). Numerical investigation of conventional and tapered Savonius hydrokinetic turbines for low-velocity hydropower application in an irrigation channel. *Sustainable Energy Technologies and Assessments*, *43*, 100871. https://doi.org/10.1016/j.seta.2020.100871

Sinsel, S. R., Riemke, R. L., & Hoffmann, V. H. (2020). Challenges and solution technologies for the integration of variable renewable energy sources—a review. *Renewable Energy*, *145*, 2271-2285. https://doi.org/10.1016/j.renene.2019.06.147

Solangi, Y. A., Tan, Q., Mirjat, N. H., Valasai, G. D., Khan, M. W. A., & Ikram, M. (2019). An integrated Delphi-AHP and fuzzy TOPSIS approach toward ranking and selection of renewable energy resources in Pakistan. *Processes*, *7*(2), 118. https://doi.org/10.3390/pr7020118

Tahani, M., Rabbani, A., Kasaeian, A., Mehrpooya, M., & Mirhosseini, M. (2017). Design and numerical investigation of Savonius wind turbine with discharge flow directing capability. *Energy*, *130*, 327-338. https://doi.org/10.1016/j.energy.2017.04.125

Thakur, N., Biswas, A., Kumar, Y., & Basumatary, M. (2019). CFD analysis of performance improvement of the Savonius water turbine by using an impinging jet duct design. *Chinese Journal of Chemical Engineering*, *27*(4), 794-801. https://doi.org/10.1016/j.cjche.2018.11.014

Thiyagaraj, J., Anbuchezhiyan, G., Mamidi, V. K., Barathiraja, R., & Sura, S. (2023). Dynamic characteristic studies of novel flexible flip-type Savonius hydrokinetic turbine. *Materials Today: Proceedings*. https://doi.org/10.1016/j.matpr.2023.03.170

Thiyagaraj, J., Rahamathullah, I., Anbuchezhiyan, G., Barathiraja, R., & Ponshanmugakumar, A. (2021). Influence of blade numbers, overlap ratio and modified blades on performance characteristics of the savonius hydro-kinetic turbine. *Materials Today: Proceedings*, *46*, 4047-4053. https://doi.org/10.1016/j.matpr.2021.02.568

Tiwari, G., Kumar, J., Prasad, V., & Patel, V. K. (2020). Utility of CFD in the design and performance analysis of hydraulic turbines—A review. *Energy Reports*, *6*, 2410-2429. https://doi.org/10.1016/j.egyr.2020.09.004

Wang, Q., Luo, K., Wu, C., Mu, Y., Tan, J., & Fan, J. (2022). Diurnal impact of atmospheric stability on inter-farm wake and power generation efficiency at neighboring onshore wind farms in complex terrain. *Energy Conversion and Management*, *267*, 115897. https://doi.org/10.1016/j.enconman.2022.115897

Wang, Q., Luo, K., Wu, C., Tan, J., He, R., Ye, S., & Fan, J. (2023). Inter-farm cluster interaction of the operational and planned offshore wind power base. *Journal of Cleaner Production*, *396*, 136529. https://doi.org/10.1016/j.jclepro.2023.136529

Wang, Q., Su, M., Li, R., & Ponce, P. (2019). The effects of energy prices, urbanization and economic growth on energy consumption per capita in 186 countries. *Journal of Cleaner Production*, *225*, 1017-1032. https://doi.org/10.1016/j.jclepro.2019.04.008

Wu, H. N., Chen, L. J., Yu, M. H., Li, W. Y., & Chen, B. F. (2012). On design and performance prediction of the horizontal-axis water turbine. *Ocean Engineering*, *50*, 23-30. https://doi.org/10.1016/j.oceaneng.2012.04.003

Yosry, A. G., Fernández-Jiménez, A., Álvarez-Álvarez, E., & Marigorta, E. B. (2021). Design and characterization of a vertical-axis micro tidal turbine for low velocity scenarios. *Energy Conversion and Management*, *237*, 114144. https://doi.org/10.1016/j.enconman.2021.114144

Zhang, Y., Kang, C., Zhao, H., & Kim, H. B. (2021). Effects of the deflector plate on performance and flow characteristics of a drag-type hydrokinetic rotor. *Ocean Engineering*, *238*, 109760. https://doi.org/10.1016/j.oceaneng.2021.109760